ABSTRACT

Design and Demonstration of an Optical Cavity-based Biosensor using Three Wavelengths to Improve Fabrication Tolerance

Caitlyn R. Breaux, M.S.

Mentor: Seunghyun Kim, Ph.D.

As diseases and cancers progress, the chances of survival depreciate; early detection is vital for improving success rates. Despite dedicated research, diagnosis has remained static—initial consultation, scanning, and then biopsies and complex immunoassay techniques are needed to receive a diagnosis. Biosensors produce a multi-faceted benefit. Early diagnosis reduces costs, saves time, and most importantly, improves quality of life. It is imperative to further develop these biosensing solutions and make diagnosis more accessible. Current diagnostic procedures require multi-million-dollar facilities, and tests are performed by highly skilled personnel. This work is dedicated to alleviating initial costs by designing and fabricating a low-cost optical cavity-based biosensor for quantitative detection at the point of care, and to provide tools to better understand bodily processes in efforts to find cures. In recent years, the optical cavity-based biosensor discussed henceforth has demonstrated high sensitivity in biosensing experiments, however the fabrication tolerance of the device itself drastically hinders the success rate of measurements. Before, the resonant changes of two

wavelengths were used in conjunction with a differential detection method for biodetection experiments. The sensitive region was limited, however, and it often involved waiting overnight for the channel to be suitable for testing. To increase usability and reduce the required time to prepare the cavity for biodetection, a third laser wavelength is integrated into the optical system to expand fabrication tolerance and reduce the channel priming time. In simulation, the third wavelength expanded the fabrication tolerance from 30 nm to 70 nm. The addition of a third wavelength was demonstrated to improve the success rate of measurements by 7% despite a larger variation in cavity width and reduce the channel priming time from 0 – 23 hours to 0 – 20 minutes.

Demonstration of an Optical Cavity Based Biosensor with Increased Success Rate Using a Three-Laser Approach

by

Caitlyn Breaux, B.S.E.

A Thesis

Approved by the Department of Electrical and Computer Engineering

Kwang Y. Lee Ph.D., Chairperson

Submitted to the Graduate Faculty of
Baylor University in Partial Fulfillment of the
Requirements for the Degree
of

Master of Science in Electrical and Computer Engineering

Approved by the Thesis Committee

Seung Kim, Ph.D., Chairperson

Linda Olafsen, Ph.D.

Jonathan Hu, Ph.D.

Jonathan Rylander, Ph.D.

Accepted by the Graduate School

May 2021

J. Larry Lyon, Ph.D., Dean

Page bearing signatures is kept on file in the Graduate School.

TABLE OF CONTENTS

LIST OF FIGURES

LIST OF TABLES

ACKNOWLEDGMENTS

I especially want to acknowledge Dr. Kim, for his time and dedication in my education and research. He provided resources, had faith in my work, and foremost of all, provided the opportunity as a summer research intern that started it all. He taught me to also keep faith in God and myself, as I learned that the path to anything worth doing is a winding one. I would also like to thank Dr. Donggee Rho, who taught and passed the torch to me in this endeavor. He set a great example in his faith, work ethic, and attention to detail. Thank you to all my professors, supervisors, and colleagues along the way whose drive, dedication, and work ethic also inspired me. Thank you to Mr. Rick and Mrs. Melissa Pardun, Mr. Alex Siller, and all my coworkers who became friends. Thank you to my committee members, teachers from the beginning and at the end of my education as an engineer—without these people writing this would not have been possible. I cherish everything I learned from them, not just about engineering, but also what it means to be a lifelong learner.

I am grateful for my family and friends; I feel fortunate to have so many at my side. I am thankful for Robbie, whose love, patience, and support has kept me grounded. I am grateful to Lauren, my sister, and Heather, Angela, and Katie, my sisters not from blood. These women saw firsthand the highs and lows and held me up through them. And lastly but not least, I am thankful for my family who molded me into the person I am today – my parents, who despite their differences still came together when it came to

raising me. Thank you to my grandmothers, who have poured prayer into my life along with their love and support.

DEDICATION

To my godmother, Pam, whose journey motivated me to work on this project, and whose faith and optimism continue to inspire me every day.

"God's got this."

CHAPTER ONE

Introduction

Despite dedicated efforts to finding a cure, incidence and mortality rates attributed to cancers have grown yearly due to greater life expectancy as seen in Figure 1 [1]. In developing countries, these rates swell to two or three times greater in developed countries [2].Therefore, in addition to finding a cure, scholars have taken to searching for easier ways to diagnose early. With lung cancer for example, the survivability drops from 63% to 7% as stages progress from local to distant locations from the lungs [3]. Not only is early diagnosis imperative to survivability, but it is also economically advantageous.

Treatment has indeed become more effective and specific with advancements such as immunotherapy and radiation. These have, however, also inflated the economic burden of treatment on the U.S. economy as incidence has risen. The initial and final costs of care are typically higher, as this includes complex diagnostic procedures and terminal phase care, respectively [4]. As of 2019, health care costs made up 17.7% of the country's GDP, growing 4.6% from the previous year. This totaled over $11,000 per capita. Current diagnostic standards boast high accuracy, sensitivity, and selectivity. However, these come at the cost of time, labor, capital, and facilities that contribute to the high economic impact. The overarching goal of biosensing is to bring diagnostics to the patient's side, or to remote areas with limited to no access to laboratory facilities.

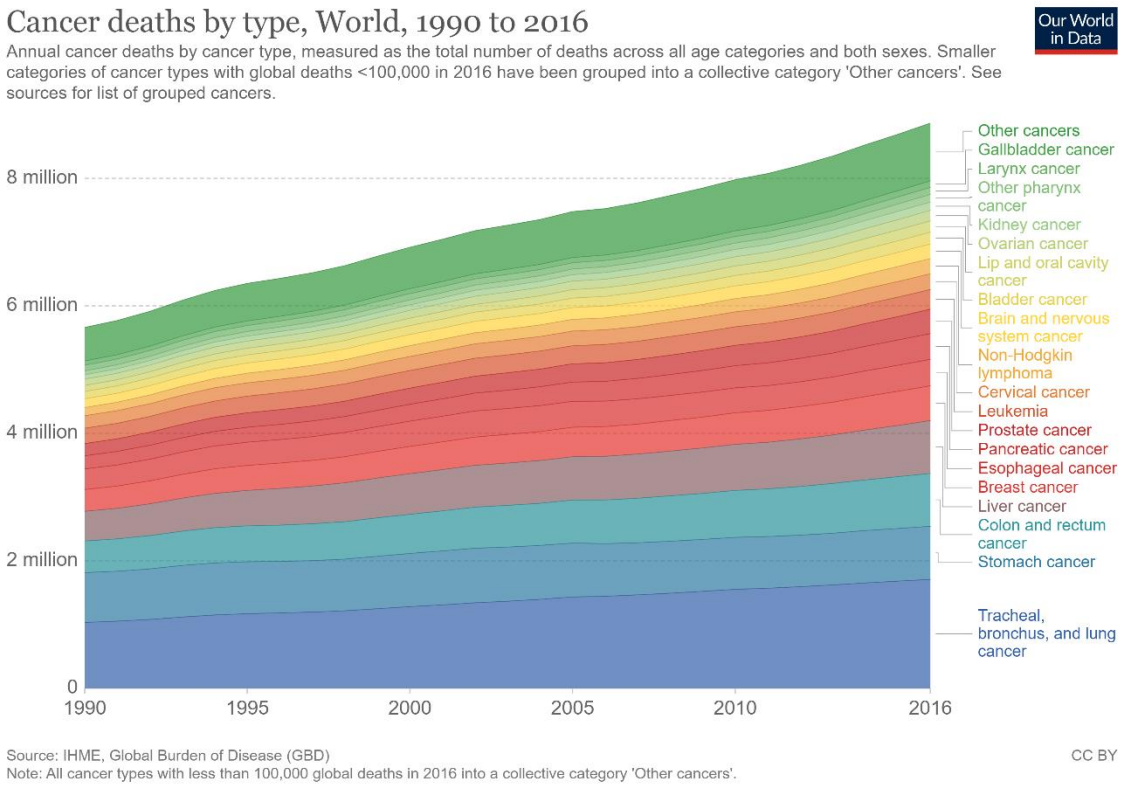

Figure 1: Growth of death rates attributed to all cancers from 1990 to 2016, from [1].

Biosensors

A biosensor marries biological recognition elements to physical transduction components to detect analytes in a test medium [5]. Biosensors may be used in environmental, industrial, and medical applications. For instance, they may be used in water quality monitoring, allergen testing in food products, and most notably in diagnosing diseases or monitoring bodily processes. The schematic in Figure 2 depicts an overview of the most notable components of a biosensor. Generally, biosensors are made up of a bioreceptor to capture analytes, and a transducer to convert reactions to electrical signals. Other data acquisition programs and equipment may be used to further process the signal. The goal of biosensing is to develop rapid, low-cost, sensitive, reliable

technology that serves as point-of-care technology to monitor conditions or provide diagnoses.

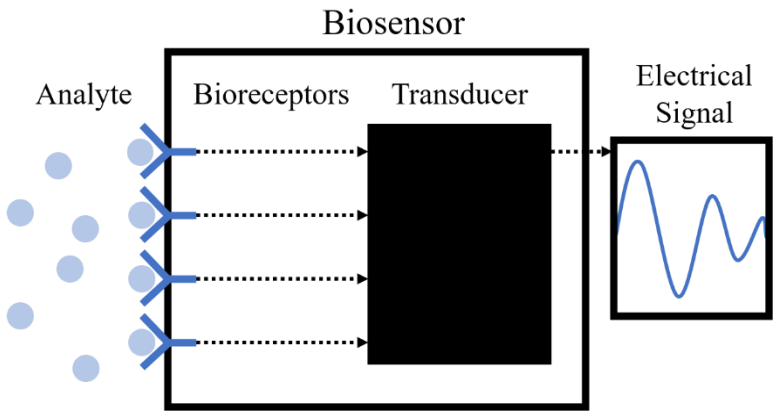

Figure 2: Overview of the general components of a biosensor.

Analytes, Bioreceptors and Recognition Elements

Analytes are biological molecules that are captured by recognition elements on the biosensor. Biorecognition elements include but are not limited to enzymes, antigens or antibodies, complementary DNA/RNA, biomaterials, polymer coatings, or otherwise affinitive elements that bind analytes to the surface of the sensor. Sensor surfaces may be prepared with a complementary receptor using a variety of processes. The analyte may be physically or chemically bonded to its recognition element [6].

Transducers

Transducers convert chemical reactions at the recognition element into electrical signals that are measurable by the rest of the system. The transduction method is the most notable differentiation between biosensors. Transducers include but are not limited to chemical, thermal, or optical types [5].

Electrochemical

Electrochemical sensors utilize the electrical signals resulting from ions created in biological reactions. These are typically categorized as sensors which use enzymes as the capture element since they are highly specific and responsive to their respective substrate. A prominent example of these is the glucose meter. Catalyzed reactions by enzymes are naturally more amplified than uncatalyzed, affinity-based reactions. However, there are limited enzyme-substrate pairs of interest that are sensitive enough for detection. These sensors may also be subcategorized by the measurement method, including current, potential, or impedance [7]. Three electrodes are used in tandem: a working electrode in contact with the reaction, a reference outside of the reaction, and in some cases an auxiliary electrode to collect potential changes from the working electrode for long-term use. Reduction-oxidation reactions cause a potential difference or current transfer between the working and reference or auxiliary electrodes. Typically these reactions happen multiple times over, like a domino effect, which lowers the limit of detection of the device [7].

Calorimetric

Calorimetric or temperature sensors rely on temperature change due to adsorption. A thermistor is coupled to the reaction medium to record temperature fluctuations. Each molecular interaction produces heat, and the heat of the medium is proportionally increased with each reaction [6].

Optical

Optical transducers convert changes in electromagnetic radiation into electrical signals. These are comprised of a light source, the optical detection element such as a prism, cavity, or fiber, and a detector to record intensity or spectral changes.

Enzyme linked immunosorbent assay (ELISA). ELISA is a standardized procedure used in medical screening, such as for HIV (human immunodeficiency virus) [8]. All ELISA types depend on passive adsorption to the well surface. ELISA well plates are commercially available in different formats that can be used in conjunction with fluorescent, colorimetric, or chemiluminescent detectors for a variety of tests [9]. Primary antibodies in direct ELISA format are simply captured by the antigen on the well surface. Indirect ELISA involves a secondary antibody conjugated with the primary antibody to enhance sensitivity, such as an avidin-biotin complex. The secondary antibody has high affinity for the primary one. The most sensitive, Sandwich ELISA, immobilizes the antigen between a capture antibody and subsequent primary and secondary antibodies with a reporter molecule to amplify the signal. The reporter molecules may be fluorescent, radioactive, or enzymatic. Each ELISA procedure involves a series of chemical introductions, incubation periods, and washes; once the reactions are complete the wells are placed in detection equipment. The resulting absorbance, fluorescence, or luminosity provides a quantitative measure of the analyte concentration present in the sample [8, 9].

Surface Plasmon Resonance (SPR). SPR-based biosensing commonly relies on either scanning a range of incident angles to find the change in resonant angle or scanning a range of spectra to find the difference in the resonant wavelength. There are several possible configurations for SPR biosensors, most notably prism (Kretschmann) and fiber in biosensing. In the Kretschmann configuration, a glass prism is coupled to the dielectric and metal films. A light source is aimed perpendicularly at the prism surface to produce total internal reflection at the prism-metal interface that is then transmitted to the detector on the other surface, as seen in Figure 3. Surface binding on the dielectric in contact with the sample medium affects the resonant angle, [10, 11].

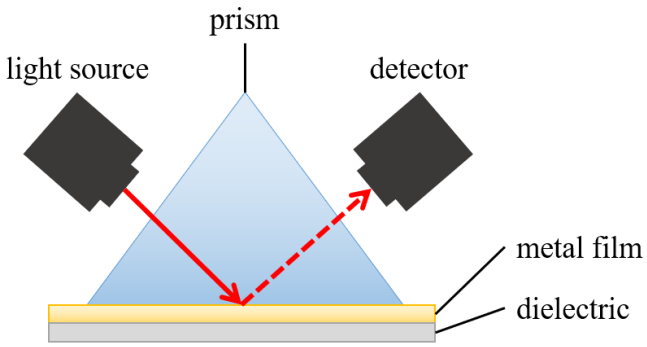

Figure 3: Schematic of SPR based sensor setup.

Fiber-based SPR utilize multimode fibers with part of their cladding replaced with metal, exposed to the medium. The operating principle is the same, with a detector and light source on either end of the fiber. Total internal reflection occurs repeatedly along the interface between the core and cladding, allowing the wave to propagate. These have a more compact form, making them suitable for miniaturization and transmission over longer distances than other configurations [10].

Whispering Gallery Mode (WGM). WGM biosensors utilize the acoustic phenomenon in which electromagnetic waves travel along a curved cavity surface of higher refractive index in a lower refractive index medium. Disturbances, such as binding events, along the surface cause phase changes due to the local refractive index change. As a result, constructive and destructive interference occurs in each round trip. In biosensor applications, these radial cavities may be affixed to prisms, waveguides, or formed on the end of tapered fibers [12, 13]. These are critically coupled via fiber or waveguide with a tunable laser, and a detector for gathering the transmitted spectra [14].

Fabry Perot Interferometer (FPI). FPI-based biosensors are simple, easy-to-fabricate resonant cavities that confine electromagnetic waves between two parallel reflective surfaces. They are easily incorporated in microfluidics, allowing for a lab-on-a-chip structure. The sample may be introduced, and interactions take place between the mirrors. Incident light enters from the source on one side, and partially reflects and transmits at each reflective interface, shown in Figure 4. When adsorption happens on one of the surfaces, the local refractive index changes, resulting in a shift in the resonant spectra [15]. The resulting transmitted intensity may be recorded by a detector on the other side, or a spectrometer may be used to determine spectral shift.

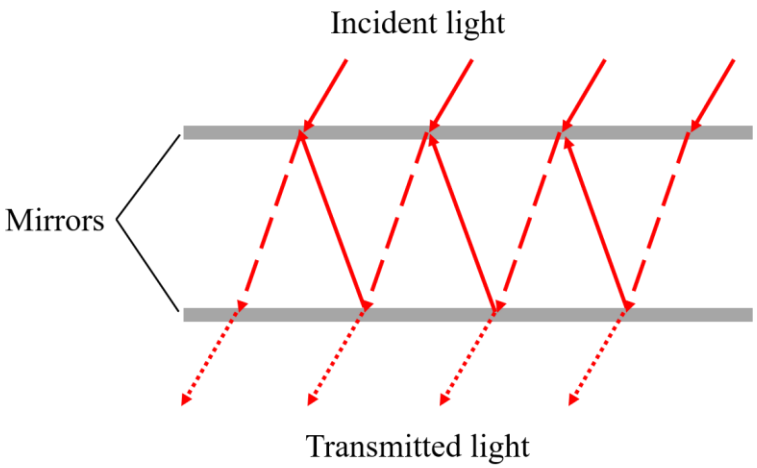

Figure 4: Schematic showing the path of light through two parallel mirrors.

In the cavity, light undergoes constructive and destructive interference; the resulting resonance curve is dependent on the resonant frequency and phase shift caused by each round trip. The frequency-dependent phase shift $\phi(v)$ for one round trip between the mirrors is given by

$$\phi(v) = 2\pi v \frac{2l}{c_n} \cos\theta = \frac{2\pi}{\lambda} 2nl \cos\theta \quad (1)$$

Where l is the cavity width between mirrors, and v is the frequency [16]. The speed of light in the medium, c_n, is the ratio of the speed of light in a vacuum to the medium refractive index, given in meters per second (m/s). Alternatively, this can be written using the wavelength, λ shown in the second half of the equation, where the refractive index is n and θ is the angle the light propagates from with respect to normal incidence [15]. When the phase shift difference between two interacting waves is an integer multiple of π, they destructively interfere. Constructive interference occurs when ϕ is equal to integer multiples of 2π.

The resulting transmittance of the cavity is given by Equation (2) below:

$$T = \frac{I_t}{I_i} = \frac{(1-R)^2}{(1-R)^2 + 4R\sin\left(\frac{\phi}{2}\right)} \tag{2}$$

Which is also the ratio of transmitted intensity I_t over the input intensity I_i. The reflectance of the mirrors is given by R. The resonant frequency, ν_m, of a cavity for a given mode, m, is determined by the following:

$$\nu_m = \frac{c_n}{2l}m \tag{3}$$

The units of frequency are determined in Hertz (Hz). Equation (3) may also be written in terms of the wavelength. The resonant wavelength, λ_m, in meters, is given by Equation (4):

$$\lambda_m = \frac{2nl}{m} \tag{4}$$

Over a range of wavelengths, there are multiple peaks in the transmission of an FPI cavity, shown in Figure 5. The separation between two consecutive peaks is the free spectral range (FSR). This is given by Equation (8) below.

$$\Delta\nu_{FSR} = \nu_{m+1} - \nu_m = \frac{c_n}{2l} \tag{5}$$

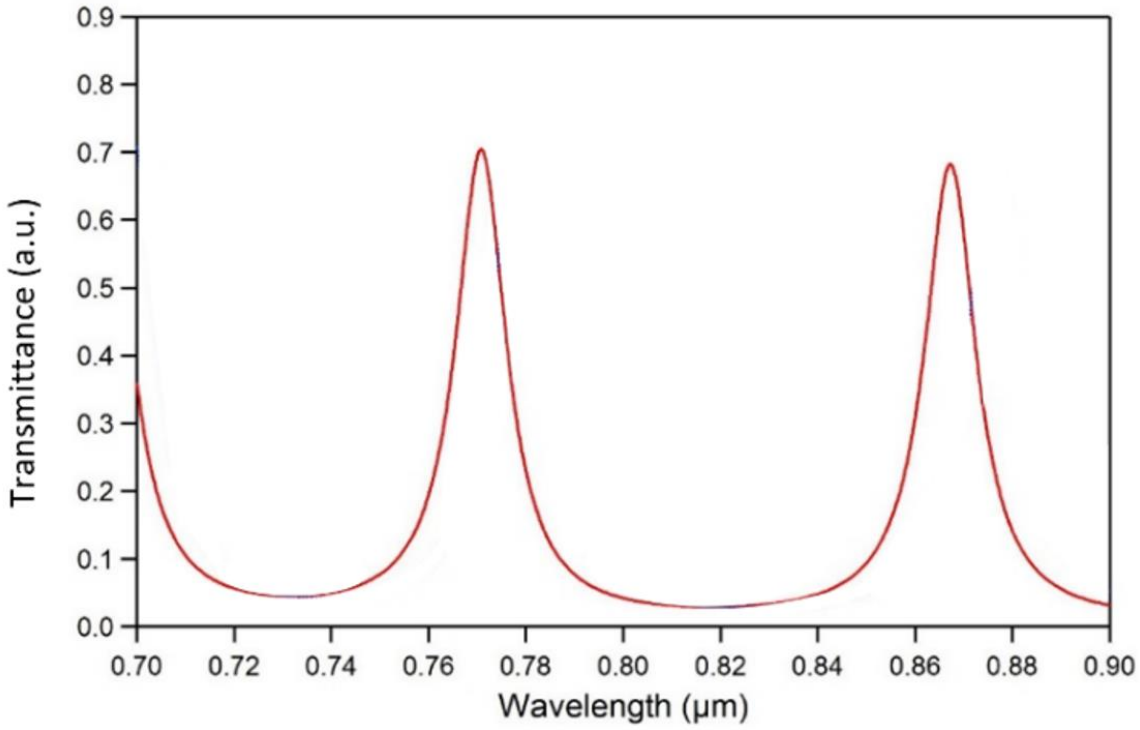

Figure 5: Transmission peaks for an FPI, from [15]. Reproduced from Open Access Article [15] in MDPI.

Labelled versus Label-free Biosensing

Biosensors may also be categorized by labelled or label-free to obtain a readable signal. Labelled reactions require additional steps to add a foreign molecule or tag to the analyte, such as fluorescent dyes. Molecules are tagged with foreign bodies in the well to create a color change proportional to the analyte concentration. Label-free sensors do not require these processes—they are sensitive and selective enough alone to obtain reliable data [17]. Resonator based biosensors and SPR are examples of label-free biosensors that are sensitive enough for detection without dyes or tags. However, these can be combined with labelling methods to further improve sensitivity.

Metrics for Biosensors

Biosensors are generally compared based on the metrics of sensitivity, and limit of detection. Optical resonator-based biosensors have an additional metric, the quality factor (Q factor). The sensitivity of biosensors is a measure of the transducer response per change in molar concentration or refractive index. The sensitivity may also be the slope of the calibration curve, or curve fitting of the response to increased molar concentration [18, 19]. For many biosensors including this work, the Sensitivity, *S*, is given by:

$$S = \frac{\Delta\lambda}{\Delta n} \tag{6}$$

Where $\Delta\lambda$ is the change in resonant wavelength, for instance, and Δn is the change in refractive index. The units are given in nm/RIU. The limit of detection (LOD) is the smallest detectable concentration above inherent noise. Typically, the LOD is given by

$$LOD = 3.3 \times \sigma \tag{7}$$

Where σ is the standard deviation of blank measurements without analytes, divided by the slope of the concentration curve. The constant preceding σ may vary between depending on the required level of confidence given by the governing entity, but in biosensor studies 3 or 3.3 are mostly used [18, 20-22]. A constant of 3 includes the probability of false positives on one tail of the distribution, with a statistical confidence interval of 95%. The constant 3.3 includes both false negative and false positive regions around the normal distribution of the sample [22].

Additionally, the Q factor in optical resonators refers to the quality of the resonance response and is given in Equation (8). The Q factor is the ratio of the resonant

frequency, v_m, for a given mode over Δv, the full width at half maximum (FWHM) centered around that frequency.

$$Q = \frac{\nu_m}{\Delta \nu} \tag{8}$$

CHAPTER TWO

Optical Cavity Based Biosensor: Two-Laser System

In previous works, the sensitivity and limit of detection of a low-cost optical cavity-based biosensor was demonstrated using two wavelengths with an FPI configuration and differential detection method. The refractive index sensitivity was demonstrated using a portable system that was created at little more than the cost of a new iPhone [23]. Later, the tabletop-based system demonstrated sensitive detection for both streptavidin and human C-reactive protein (CRP) [24].

Fabrication and Test Setup

For the tabletop optical system, all components are affixed to a stabilized optics table, and are mounted using Thorlabs mounting posts and fixtures. Two visible range (near-IR) laser diodes of different wavelengths were arranged perpendicularly to a 50:50 beam splitter to combine the beams. The beams also pass through a neutral density filter before the mirror to attenuate the laser power, avoiding saturation at the camera. The lasers are directed at the cavity in turns by a beam blocker connected to a servo that alternates positions around the beam splitter. The unblocked beam shines through the cavity and out toward the CMOS camera, positioned on the opposite side of the cavity structure (Figure 6a).

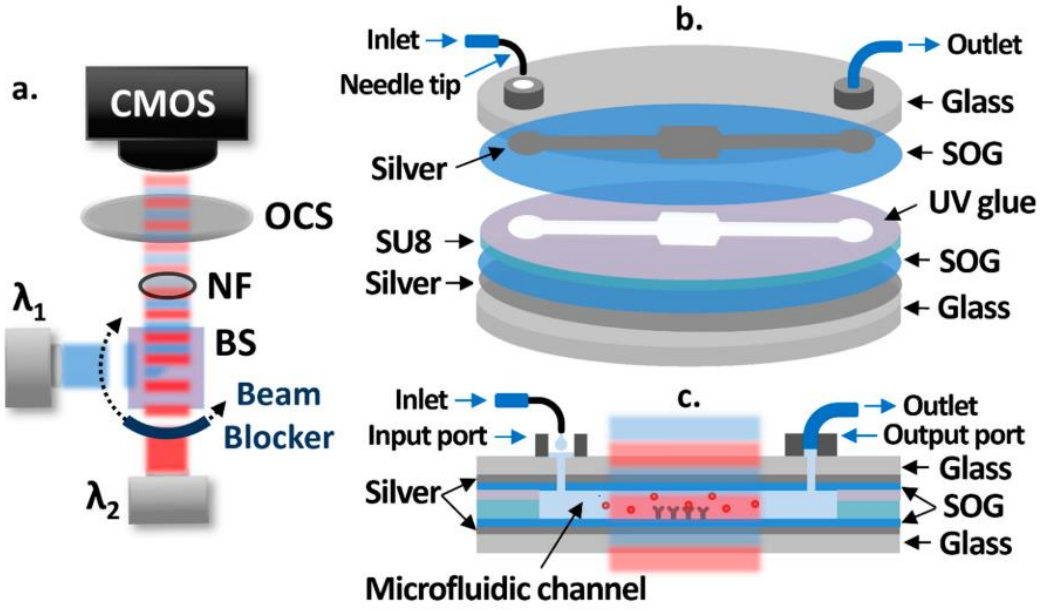

Figure 6: (a) Two-laser system setup, (b) microfluidic channel schematic and (c) binding interaction overview as seen in Rho *et al*., 2020. Reproduced from Open Access Article [24] in MDPI.

The resonant cavity structure (which doubles as a microfluidic channel) was fabricated through a series of thin film deposition processes. The partially reflective, 20 nm-thick silver mirrors were sputter-coated onto glass substrates, then covered with a densified spin-on-glass layer of 400 nm. The channel floor was functionalized specifically for subsequent bio-detection tests. For fluid tests, the openings for the channel were connected to 3D-printed input and output fixtures for fluid introduction and evacuation. The adapted optical cavity (Figure 6b) was then placed in alignment with the lasers' path and CMOS camera. Fluid introduction was done using a syringe pump at the inlet, and fluid was removed using a micropump at the outlet (Figure 6c).

Differential Detection Method

As demonstrated in previous papers, the differential detection method amplifies the sensitivity of the measurements compared to either resonant response alone [24-26]. It was previously demonstrated to mitigate common noise in the resonant curves while improving the responsivity multiple times in both the tabletop and portable systems [23, 25, 27]. Since inception, however, the differential equation evolved into the current version, depicted in Equation (9).

$$\eta = \frac{I_1 - I_{10}}{I_{10}} - \frac{I_2 - I_{20}}{I_{20}} \tag{9}$$

The differential value, η, is derived from the difference in intensity changes scaled by the original respective intensity of each laser. I_1 and I_2 are the intensities after a time period, while I_{10} and I_{20} are the initial intensities for the respective wavelengths [28]. The differential detection method is consistent between the two and three laser systems detailed in this work. Biorecognition capability using the differential method was previously demonstrated on an optics table using streptavidin and biotinylated BSA. As the sensing layer thickness increased, the two laser wavelength intensities diverged; the differential between these two opposite changing intensities was shown to provide a higher sensitivity than either alone by a factor of ten [28].

When using the differential detection method, it is imperative that the two transmitted intensities are changing in opposite directions, also known as the measurement condition. The differential is negative when the two are the same sign, and positive when they are not. I_1 should be increasing in transmitted intensity while I_2 should be decreasing, to maximize the differential value.

Polymer Swelling

Not long into the process of performing the tests, it was evident that the swelling of SU8 polymer used to form the channel walls affected the resonant response but was unavoidable, since the moisture from fluid tests was always present. When SU8 films are exposed to moisture, the stiffness is lower at room temperature. Polar water molecules are attracted to the polar molecules in the epoxy [29]. As a result, the thickness of SU8 and the gap between the two SOG layers widens over time with exposure. This swelling property was cleverly used as a priming mechanism to wait for the measurable conditions (i.e. the crossing of two oppositely changing resonant curves) [24]. The cavity samples were also fabricated slightly smaller than the ideal cavity width of 8 μm to accommodate that swelling, to increase the chances of reaching the point where two intensities change in opposite directions. This accounts for some deviation in cavity width occurs from one channel to the next; there is still an opportunity for the channel to be usable. After about 20 hours however, the SU8 saturates with water, and the channel swelling slows drastically, limiting the swelling amount. Using measurements of the cavity width before and after testing, the approximate swelling rate was determined to be 0.11 nm/min for the two-laser design. The amount of swelling needed to reach the measurement conditions ranged from 0 to 23 hours, and the maximum swelling amount derived from the 23-hour swelling time was 96 nm. The combined average swelling rate was around 0.11 nm/min. The measurable window is about 30 nm once it begins, or about 270 minutes (4.5 hours). However, the swelling rate is not consistent over time. As the availability of polar groups declines, we expect that the rate of reaction is slowed, and the cavity walls saturate with water. This behavior is explained further in Chapter 5, Swelling to Reach Measurement

Conditions. The swelling effects are compensated for in the intensity measurements, and the changes due solely to bio-interactions were extracted.

Sensitivity and Limit of Detection Experiments

To demonstrate device sensitivity, a basic streptavidin-biotin assay was used. Streptavidin and biotin are proteins with high affinity for one another, thus they are commonly used as test molecules in biosensing to demonstrate sensitivity in literature. In commercial assays, such as in ELISA, streptavidin or avidin-coated wells are used to efficiently capture biotinylated molecules whose passive adsorption is not as efficient [9]. Deionized (DI) water is introduced first into the functionalized microfluidic channel to begin swelling. Once two laser intensities began sloping in opposite directions, the test began. Different concentrations of streptavidin in DI water were introduced for preliminary detection tests, and then DI water to rinse unbound molecules. Figure 7 depicts the cavity response to streptavidin, after the linear changes due to swelling were separated from the data.

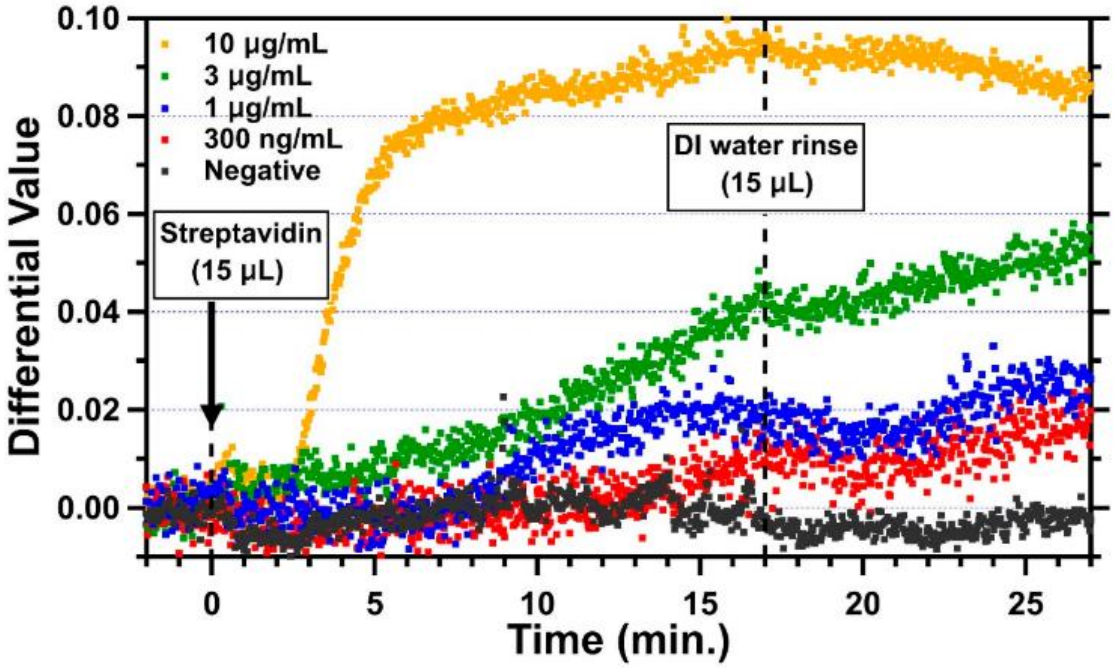

Figure 7: Compensated differential responses to various concentrations of streptavidin. Reproduced from Open Access Article [24] in MDPI.

CRP is an inflammatory biomarker whose concentration in blood spikes in response to severe infections, heart disease and autoimmune disorders [30, 31]. Biotinylated CRP antibody was introduced to streptavidin-prepared channels. For CRP detection, a slightly different sequence was performed. Once measurement conditions were met, streptavidin was first immobilized on the biotinylated channel floor, incubated, and then DI water was used to rinse away unbound streptavidin. Then biotin-conjugated CRP antibody was injected and incubated, then subsequently rinsed, which serves as the receptor molecule for CRP. This conjugate antibody is captured by streptavidin from the preceding step due to the high affinity of streptavidin and biotin. CRP- spiked tris-HCl buffer was introduced and allowed to incubate. The channel was then rinsed with DI water as in preceding steps. Logarithmic concentration curves were developed for both.

The two-laser optical cavity biosensor resulted in limits of detection (LOD) of 71.3 ng/mL (1.35 nM) for streptavidin and 43.3 ng/mL (56.4 nM) for CRP which is well below what is considered healthy by clinical standards [24, 31].

Room for Improvement using a Third Laser Wavelength

One drawback of the two-laser system is that the swelling (priming) period could take up to 23 hours. The data in

Table 1 was gathered using our research group's internal database, where the swelling and test times were recorded in addition to processed test data used in the paper. Out of 16 tests attempted, pre-test swelling time to reach ideal conditions could vary between 0 to 23 hours, with an average of 7.71 hours. The detection test time counts the time from when streptavidin is first introduced to when the DI water rinse leaves the channel, and a second rinse is introduced. The average detection test was around 34 minutes. In addition, the success rate was limited by the scope of possible resonant activity during that swelling period. In these samples, if the channel swelling did not reach a measurable condition over 24 hours, it was considered unusable. The measurable condition considered throughout these works is where two wavelengths exhibit oppositely changing intensities. The success rate (in percent) is the number of channels usable for detection tests out of the total number of channels fabricated during the time of working on the previously mentioned publication from 2020. The success rate of achieving the measurable conditions in these samples was 81%, or 13 of 16 samples.

Table 1: Metrics from the most recent two-laser system detection tests.

Parameter	Average ± one standard deviation
Priming Time (hours)	7.71 ± 6.92
Detection Test (minutes)	34.62 ± 5.32

The aim of adding a third wavelength to this design is to expand the fabrication tolerance to increase the success rate of cavity samples. Doing so widens the time and cavity size window usable for biodetection. The additional wavelength reduced the cavity swelling time in turn as well, and all tests were completed in under an hour. In the following chapters, the effects of adding a third wavelength on fabrication tolerance and success rate is demonstrated.

CHAPTER THREE

Three Laser Optical Cavity-based Biosensor

In recent tests using the two-laser optical cavity-based biosensor, the need for additional fabrication tolerance is evident, to reduce test time, materials used, and increase the success rate of samples. It is imperative that in these stages of development that fabrication is made easier and more successful to conserve time and resources long-term. While the sensitivity was clearly demonstrated, the fabrication tolerance is narrow, hence the need for long swelling tests to achieve measurement conditions. In addition, one of the tenets of Point-of-care (POC) biosensors is to be rapid. Overcoming the need for swelling time fulfills that tenet, while the low-cost and sensitive qualities have been demonstrated before. The search for the third wavelength began with the two-wavelength cavity design.

The following simulations were performed using an optical device simulation software (FIMMWAVE/FIMPROP). First an exploratory simulation was performed with a fixed cavity size with refractive index 1.3 to 1.4 to determine which wavelength to add to the current two laser design, whose simulation is shown in Figure 8. The wavelengths considered were in the visible, near-IR range to maintain low device cost. The upper refractive index limit of 1.4 covers the range of refractive indices possible due to the formation of thin layers of proteins, cells, and other biological analytes, such as a streptavidin-biotin complex, seen in literature [32, 33]. Much of the cavity width would be filled with buffer solution (RI 1.333), so the expected range is centered around 1.33.

The parameters set for the three-laser design were transferred from the basis of the two-laser design. The silver thickness was 20 nm, the glass substrate thickness was 500 nm, the cavity width was set to 8 µm, and the SOG layer was set to 400 nm. Any two wavelengths' efficiencies should change in opposite directions for the differential detection to work. This is referred to as the measurement condition. The design showing a set of peaks with measurement conditions beginning at 1.33 was determined, since that is the refractive index of the DI water, the first fluid introduced to the cavity during tests. The range up to 1.4 encompasses the refractive index of our stock solution of streptavidin in DI water (1 mg/mL, or 18.2 µM), which is 1.335.

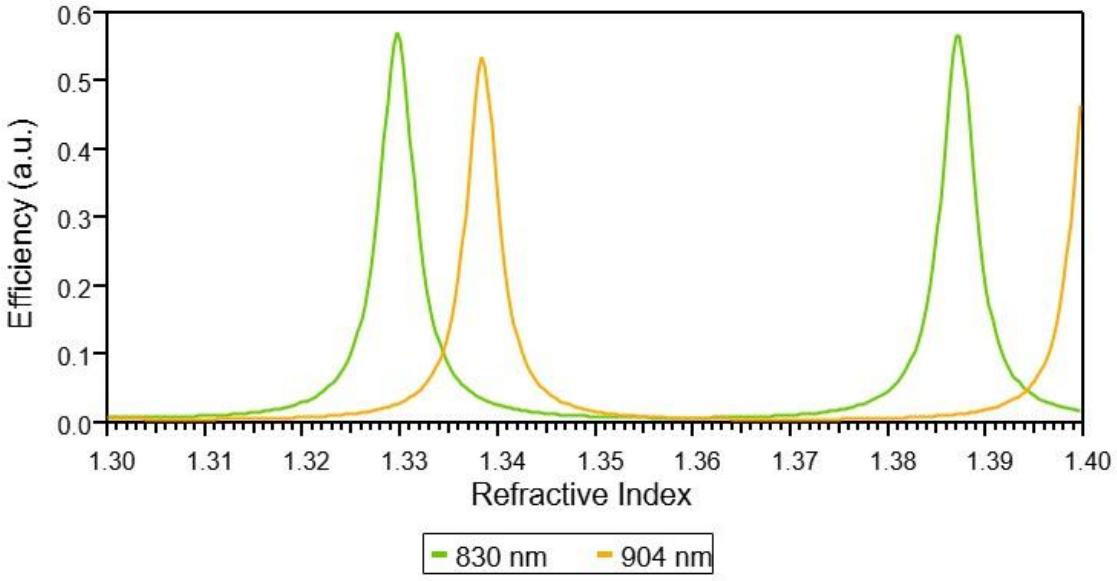

Figure 8: The resonant response of the two-laser system for a cavity width of 8 microns, with the first peak of 830 nm decreasing while the 904 nm increases starting at 1.33 RIU.

A third laser wavelength of 808 nm (blue) was chosen since its resonant curve overlapped with the 904 nm (gold) laser with similar spacing to the 830 nm (green) and 904 nm pair, as shown in Figure 9. In addition, this wavelength was chosen over the

possible 780 nm or lower wavelength lasers. Losses and round trip phase shift inherent to resonators like these are dependent on frequency [16], along with the transmittance. Therefore, to produce a cavity design that transmits the greatest efficiency for all three, it is more practical to use similar frequencies. As seen in Figure 9, at the refractive index of DI water (1.33) the 830 and 904 resonant peaks overlap. As the refractive index increases during adsorption, the 830 nm efficiency decreases while the 904 nm efficiency increases. The additional wavelength, after 904 nm provides more ample opportunity for the cavity to be used if the fabricated device is slightly larger than the ideal design.

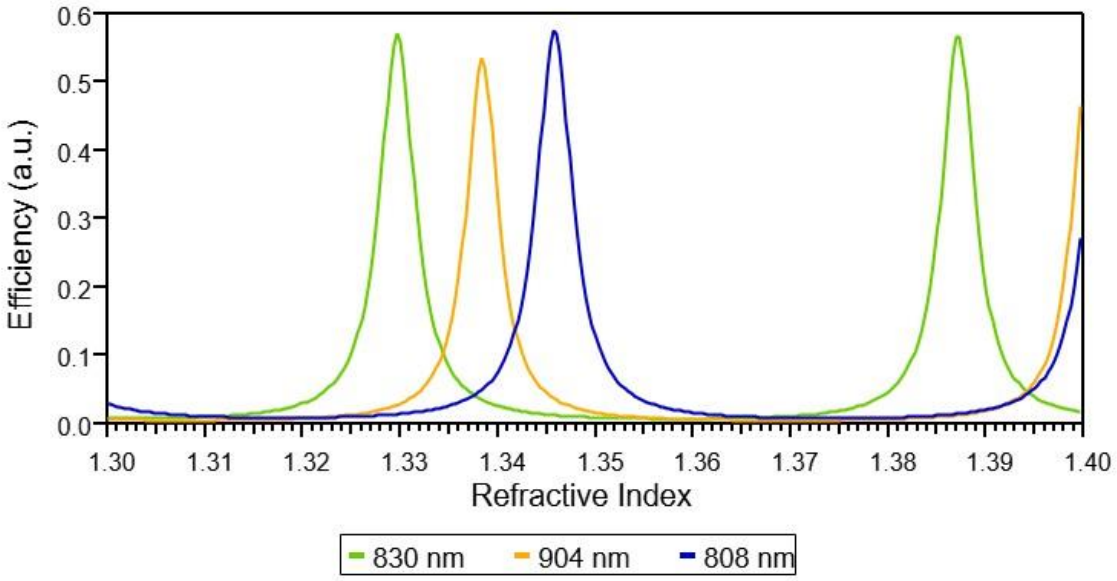

Figure 9: Addition of a third wavelength, 808 nm, to the two wavelengths in the previous design.

The efficiency for the select group of lasers was simulated in response to refractive index changes and repeated them for varying cavity widths from 7.95 to 8.15 microns. Using these simulations, the ideal cavity width was determined based on if the linear responses were present in the refractive index range of fluid used for the test

(1.3329 – 1.3345). For the target cavity width, either of the two crossing ranges should be present or could be reached with the inherent swelling of the SU8 cavity. The swelling rate drops exponentially after some time, so it is imperative the cavity is smaller or at a measurable condition. The ideal cavity width was kept at 8 microns, since the first wavelength peak, 830 nm, appears at 1.33 RIU.

Fabrication Tolerance

To determine the fabrication tolerance, a separate simulation of the efficiency response to sensing layer growth was conducted. The efficiencies of all three wavelengths were found in response to sensing layer growth, while the cavity width was fixed. The efficiencies for 0-20 nm uniformly thick sensing layers were found using a refractive index of 1.45 for the sensing layer. This thickness was assumed to include variation in streptavidin molecule sizes for biodetection tests, which can occur upon adsorption [34]. The differential value is demonstrably more sensitive than either efficiency response alone. For the ideal cavity width of 8 μm, the 830 nm wavelength efficiency is expected to decrease from 0.180 to 0.137, and the 904 nm efficiency increases from 0.063 to 0.077 (Figure 10). In this cavity size, the 808 nm efficiency does not significantly change, but does increase from 0.02007 to 0.02162. Relying on the change of either efficiency at a single wavelength is not as responsive as the differential method, which linearly increases from 0 to 0.544. For any given cavity width, the differential retains its sensitivity even when the efficiencies are low, as shown in Table 2.

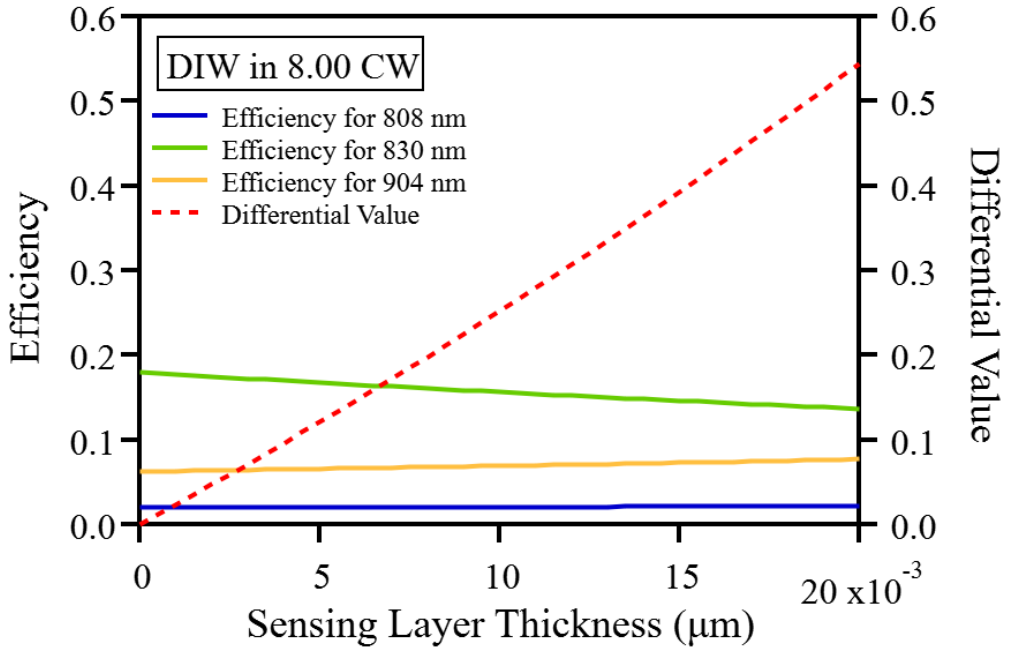

Figure 10: The efficiencies for 808 nm (blue), 830 nm (green), and 904 nm (gold) wavelengths. The differential response for the 830 nm and 904 nm pair is shown also, as a dashed red line.

Table 2: Efficiency changes for each wavelength alone, versus differential change over 0-20 nm sensing layer growth.

830 nm	904 nm	808 nm	Differential
- 0.043	+ 0.014	+ 0.0016	+ 0.544

To determine the fabrication tolerance, the differential calculation above was performed for increments of 10 nm for a range of cavity widths from 7.95-8.15 µm. Figure 11 shows the differential values for this range. At each cavity width, the differential calculation was performed if there were two oppositely changing efficiency curves. There were no oppositely changing efficiency curves (measurable conditions) for ranges 7.95 to 7.98 µm and 8.07 to 8.15 µm; thus these ranges are not shown. The data points in red are the range of cavity widths measurable by the two-laser system, with only 830 and 904 nm wavelengths. The data point in blue is the result of using the 830 and

808 nm wavelengths at 8.03 µm, where the 904 nm wavelength reaches a peak with 0 slope. The ranges 8.03-8.06 utilize the 904 and 808 nm wavelength combination, shown in green. Overall, the fabrication tolerance estimated from Figure 11 for the two-wavelength design is 30 nm, or from 7.99 to 8.02 µm. The approximate fabrication tolerance for the three-wavelength design is 70 nm – more than double that of the two-wavelength design – 7.99 to 8.06 µm. Therefore, to greatly improve the device success rate by increasing the fabrication tolerance, a third wavelength at 808 nm is incorporated.

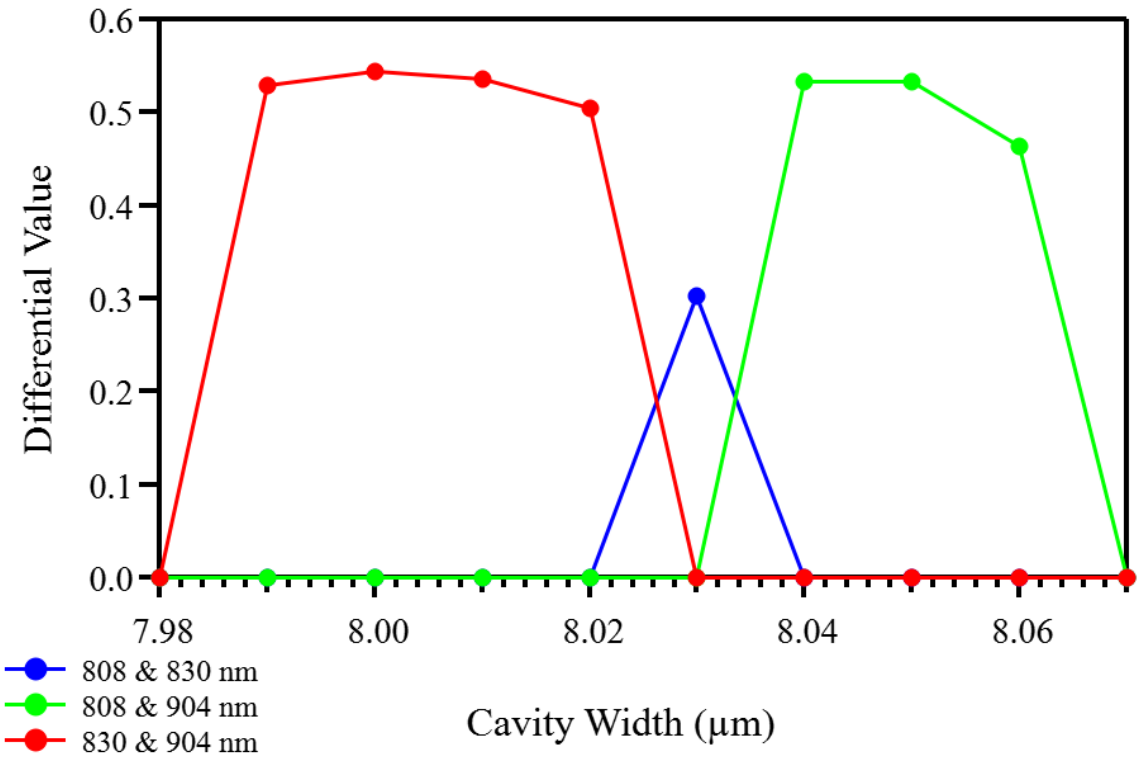

Figure 11: The differential values at 20 nm thick sensing layers for cavity widths of 7.95-8.10 µm.

CHAPTER FOUR

Experimental demonstration of Three Laser Optical Cavity-based Biosensor

To prove the three-laser design will improve the fabrication tolerance and reduce overall test time, swelling tests and streptavidin detection tests were conducted. The fabrication process largely remained the same as for the two-laser design. The differential response of the three-laser system was compared to that of the two-laser system for streptavidin detection.

Fabrication

First, two glass substrates are cleaned. On one, four 1-mm holes are drilled to create inlet and outlet openings for two separate channels. Then silver is sputtered for 15 seconds using a Torr DC sputterer at 100 W. AZ is spin-coated onto it at 2000 RPM, then exposed to UV under a photomask for 95 seconds. The mask (Figure 12) is patterned to leave silver in areas where the channel would be and leave plain glass around it. The mask design contains two channels about 50 mm long, including their 2-mm wide inlet and outlet areas. The inlet and outlet areas are the circular sections on the left and right-most ends which are used to align the drilled holes with the channel. They are slightly larger than the 1mm drilled holes to account for variations in position from manually drilling into the glass. In the center, the channel tapers outward from 0.5 mm wide to 1 mm wide, to create the sensing area. The sensing area is about 3 mm long and 1 mm wide between the tapered ends.

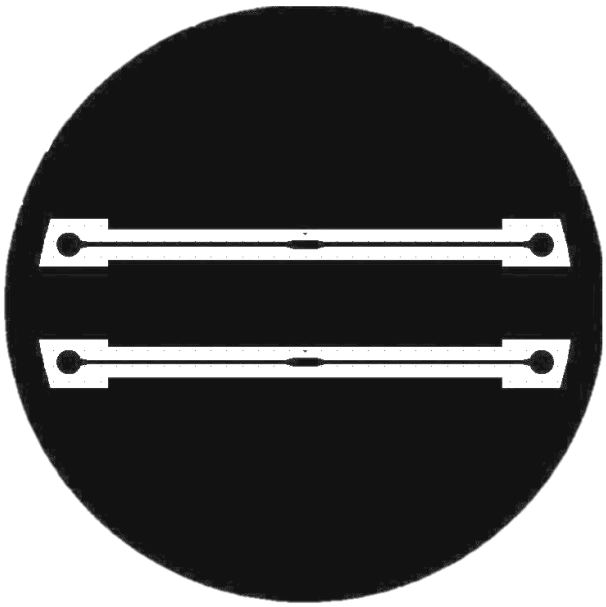

Figure 12: Mask Design used to create channel structure.

Then silver is etched from the white areas in Figure 12, and spin-on-glass (SOG) is spun onto it at 1200 RPM. The solvent from the spin on glass liquid is then evaporated by baking it on a hot plate at 130°C for four minutes, and cooling slightly at 100°C for four minutes to prevent cracking from drastic temperature changes. Then it is densified by RF-sputter coating silicon dioxide (SiO_2) for 10 minutes at 100 W, using the procedure outlined in [35]. After the SOG is densified, the drilled substrate (top section of Figure 13) is then treated with oxygen plasma to form hydroxyl groups on its surface needed for silanization using (3-Aminopropyl)triethoxysilane (APTES, Sigma Aldrich); the process is based on the procedure in Zhu, *et al*. [36]. The substrate is placed in a desiccator with vaporized 0.5 mL 99% APTES on a 90°C hot plate. After incubating in vaporized APTES for 24 hours, the substrate is then rinsed in an ultrasonic DI water bath for 7 minutes to remove unbound or excess APTES molecules. A monolayer of APTES is ideal for silanization, to generate a uniform layer of amine groups for the next step. After

drying with nitrogen, the layer is annealed on a hot plate at 110°C and then allowed to cool for 1 minute. N-Hydroxysulfosuccinimidobiotin (Sulfo-NHS biotin, 5 mg/mL in DI water) is dropped in the sensing area, to create a biotinylated surface. Bovine serum albumin (BSA, 1% in DI water) is used to passivate the rest of the channel pattern. The substrate is then incubated in a humid, closed container for 1 hour and subsequently, rinsed with DI water and dried with nitrogen.

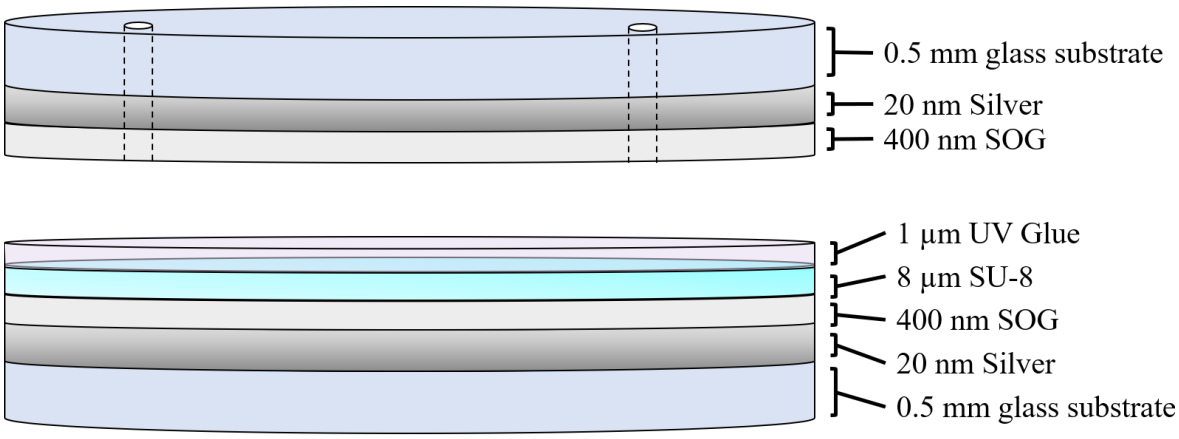

Figure 13: Schematic of the device fabrication process. Two drilled holes (as opposed to the actual 4) are shown for simplification in the top substrate, which provide access for fluids to be introduced or removed. The subsequent layers formed on each glass substrate are shown. After stamping UV glue, the two parts are glued together to enclose the channel.

The other, undrilled substrate is also sputtered with silver, but not etched. The SOG is spun on and densified after as well. To form the channel walls, an SU8 pattern is spin-coated at 1100 RPM, baked on a 95°C hot plate for 3 minutes, and exposed under a mask in UV for 130 seconds. The SU8 then undergoes a post exposure bake at 95°C for 3 minutes, followed by developing in SU8 developer for 1 minute and dying with nitrogen. The channels formed are then passivated with BSA using the same procedure as that of the drilled substrate. Once both are prepared individually, they are bonded together using

UV glue. The UV Glue is spin coated at 12,000 RPM onto a transfer wafer. The wafer is lightly cured under UV for 400 seconds to thicken the glue to prevent it from bleeding into the channel when transferred. The SU8 surface of the plain substrate is stamped with UV glue, and then quickly bonded with the drilled substrate, in the orientation shown in Figure 13. They are cured together for 3 hours in a UV box. The SU8 channel walls on the undrilled side are then enclosed by the flat SOG surface of the drilled substrate. 3D-printed inlet and outlet ports are affixed to the drilled holes. Fluids may then be introduced to or evacuated from the microfluidic structure at the drilled holes, such as in the excerpt below from Figure 6c. As in the two-laser system setup, the inlet port is open, filled with consecutive liquids from the syringe pump. The outlet is enclosed by tubing connected to a vacuum pump to remove fluids from the channel.

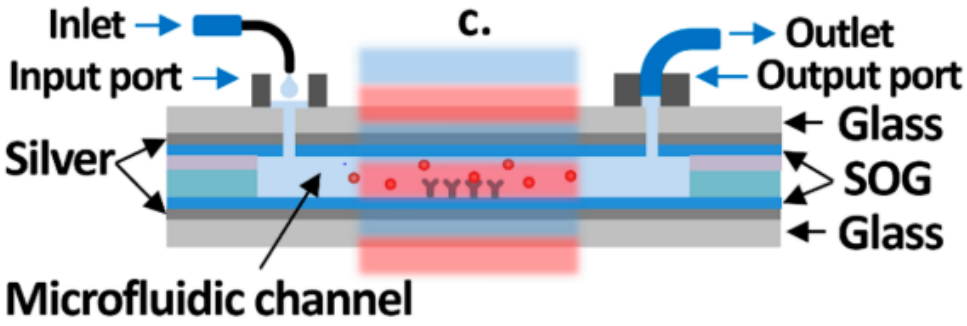

Figure 14: Excerpt from Figure 6, a cross sectional view of the channel, inlet and outlet port setup.

Optical System Setup and Tests Performed

Fluids are introduced to functionalized channels which are composed of two mirrors. This allows partial transmission and reflection of light from specific wavelengths of inexpensive laser diodes. As the refractive index changes, the transmission from the

cavity for each laser changes. A CMOS camera collects images of the channel which are processed further using a computer. The three beams are combined using beam splitters and their intensities are attenuated using a neutral density filter to avoid saturation in the images collected. A mirror then directs the alternating beams upward to the cavity, to the CMOS camera. There is a rotating blocker connected to a servo that is positioned above the 830 nm and 808 nm beam splitter to alternate which is allowed through. The same goes for the other servo blocker dedicated to the 904 nm. The 830 nm laser was placed on the 30% ratio side of the 70:30 beam splitter to compensate it having double the power output of the other two. This way, the intensities are more balanced. Fluids are dropped in the input port in the same fashion as the two-laser system: a syringe tip connected to a syringe pump via tubing is positioned just a few millimeters above the port opening. Fluids are introduced consecutively, before the port empties, to avoid air gaps between fluids. A micropump pulls fluid through the channel through the tubing connected to the 3D-printed output port on the sample.

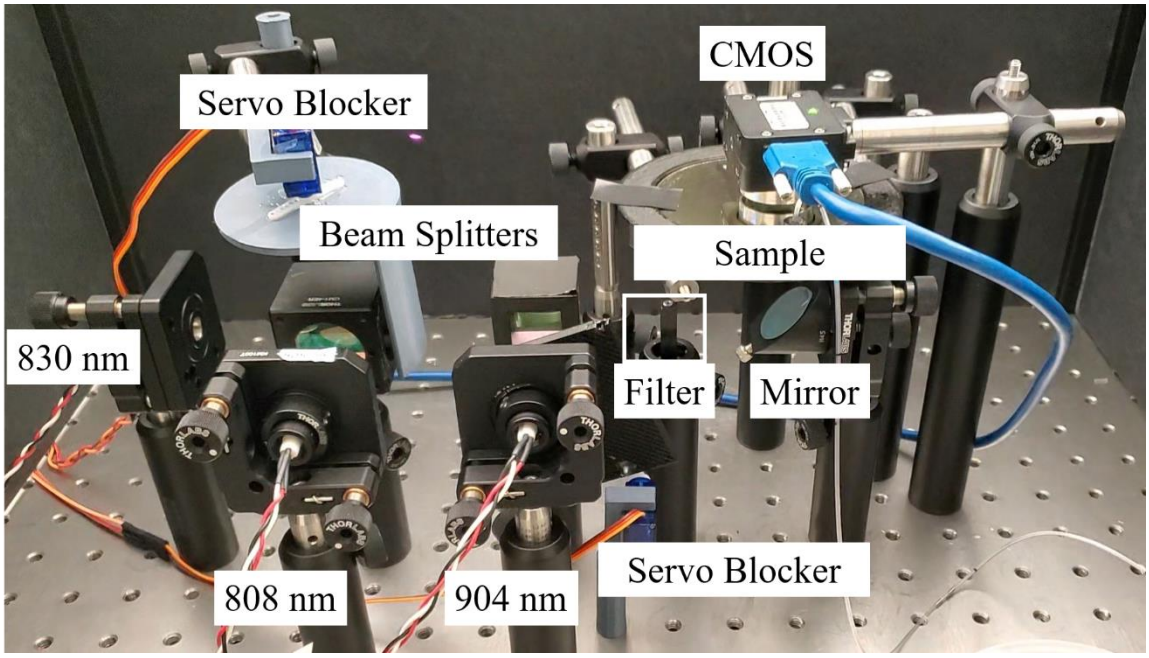

Figure 15: Three-laser system used for testing the optical cavities.

Swelling to Reach Measurement Conditions

Using a third laser wavelength was expected to increase these chances of approaching a measurement condition within 20 hours, since the fabrication tolerance was doubled. After 20 hours, the intensity changes appear to slow, indicating the cavity possibly becomes saturated around that time. An example of this is shown in Figure 16. DI water was introduced and the vacuum was left on for a period of 20 hours with no intervention otherwise. If the swelling rate were constant, the other side of the 808 nm peak would have been observed. Since it was not, it can be assumed that the peak intensity was sustained due to there no longer being a swelling cavity. In this respect, the three-laser system performed better than expected by reaching measurable conditions within 20 minutes for 7 of 8 samples.

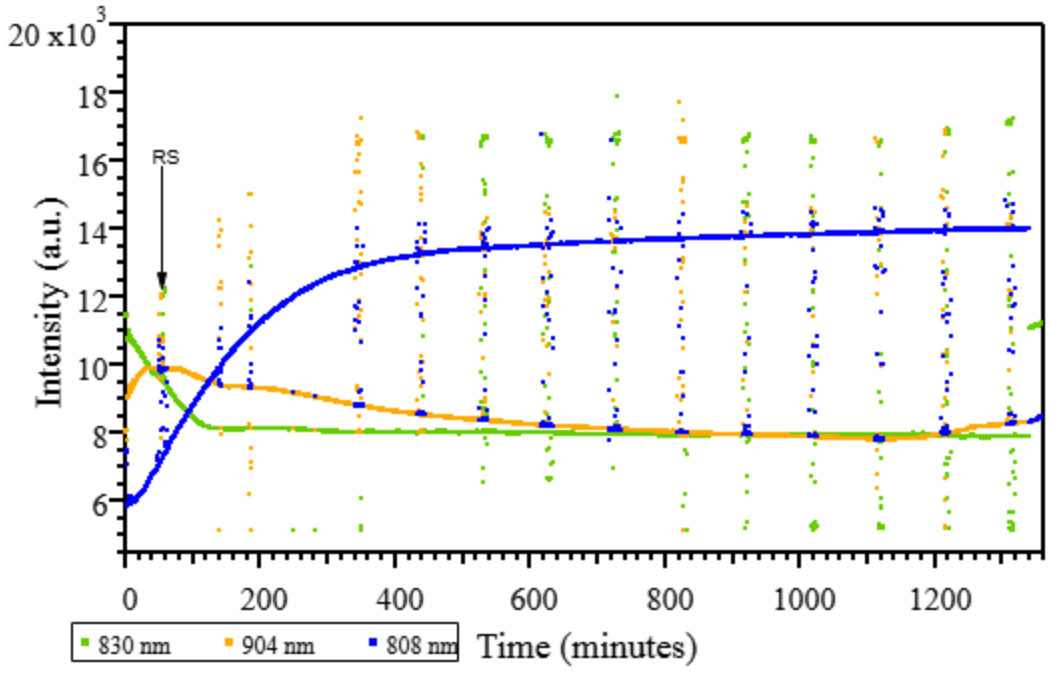

Figure 16: Swelling test of over 20 hours, showing the intensity leveling off at 14000 for 808 nm, and the other two remaining in the valley for most of the test.

There are some points in tests when the timing of the servos is not synchronized with the camera recording images. At those points the camera recording must be reset and started when the lasers are not being blocked. These points are indicated in the following by “RS”, the abbreviation for “resynchronized”. In Figure 16, the camera had to be resynchronized multiple times over the period of 20 hours. When left unsupervised, the timing cyclically returns to recording the wavelengths switching on time, and then again devolves to recording the transition between two wavelengths every 100 minutes.

The data in Table 3 below are the swelling times, and their approximate cavity widths (CW) using a third wavelength. The swelling time is the time it takes to have two intensities changing in opposite directions after the first introduction of DI water in the cavity. In one test, the swelling test was terminated after two hours. An air bubble grew in the sensing area, making the intensities change erratically, so it could not be

determined whether that sample would reach the measurement condition. It is important that the channel remains filled with fluid throughout tests to prevent inconsistent swelling and interruptions in the sensing area such as this.

Table 3: Swelling times and cavity sizes for 8 cavities.

Cavity Sample (N)	Swelling Time (minutes)	Post Test CW (μm)
1	5	8.47
2	Indeterminate	8.44
3	20	8.99
4	0	8.18
5	0	8.18
6	0	8.00
7	0	8.36
8	10	8.30

The post-test cavity widths were measured using a contact profilometer (Alpha-Step D-500, KLA Instruments). The fabrication error was 990 μm. The large variation may be attributed to a combination of fabrication errors such as irregularities UV glue height, or to the variation in swelling and test times. The swelling measurements also depend on the amount of time the sample was empty before measurement, allowing it to dehydrate and shrink. Therefore, the exact CW at the time measurable conditions are met cannot be determined.

The success rate was increased from 81% to 88% using a third laser wavelength, and the priming (swelling) time average was reduced from 7.71 hours to just 4.29 minutes. The swelling time ranged from 0 to 20 minutes instead of 0 to 23 hours. below is a tabulated comparison of these parameters for the two- and three-laser wavelength designs. Despite a larger fabrication error, the success rate using a third wavelength was higher.

Table 4: Swelling time and success rate comparison of the two systems.

Parameter	Two-Laser System	Three-Laser System
Priming Time	7.71 hours	4 minutes
Fabrication Error	107 nm	990 µm
Success Rate	81%	88%

Streptavidin Detection Tests

Next, the differential response to a streptavidin concentration of 10 µg/mL was determined to compare it with the two-laser system. This test was to ensure that the larger fabrication tolerance was also just as efficient for molecular detection, not just speeding up the test time. A simple biotin-streptavidin complex test was conducted using two samples (6 and 7 from Table 3 above). Each point is the average pixel intensity of a 150 µm × 150 µm area (0.0225 mm^2). Cavity expansion affects the average pixel intensity, as does the adsorption of streptavidin (STV) to the biotin-coated surface of the channel. In Figure 17 depicts a test conducted for one of the cavities, 8 µm wide after the test. The measurable conditions were seen immediately. The 808 nm (blue) intensity is reduced from 41,783 to 23,111 over the 30-minute window shown. The 830 nm (green) intensity increased from 8,256 to 11,537. The 904 nm intensity (gold) is flat, indicating it is in the valley between two peaks. The 808 nm and 830 nm intensities were used in the differential calculation, shown in red. The differential minus the swelling response, otherwise known as the compensated differential value, is shown in light blue. When streptavidin is introduced at 14 minutes, the compensated differential value increases from 0.55 to 0.75, indicative of the combined bulk and local refractive index changes. After 10 minutes, DI water is introduced to rinse unbound streptavidin and only local refractive index changes due to the sensing layer remain. After at least 25 minutes of

incubation the differential change was determined. The 0.228 differential increase from 0.557 to 0.785 was due strictly to streptavidin adsorption. After DI water is introduced at 26 minutes, the compensated differential still shows some latent increases, possibly due to rinsed streptavidin molecules re-attaching in other areas.

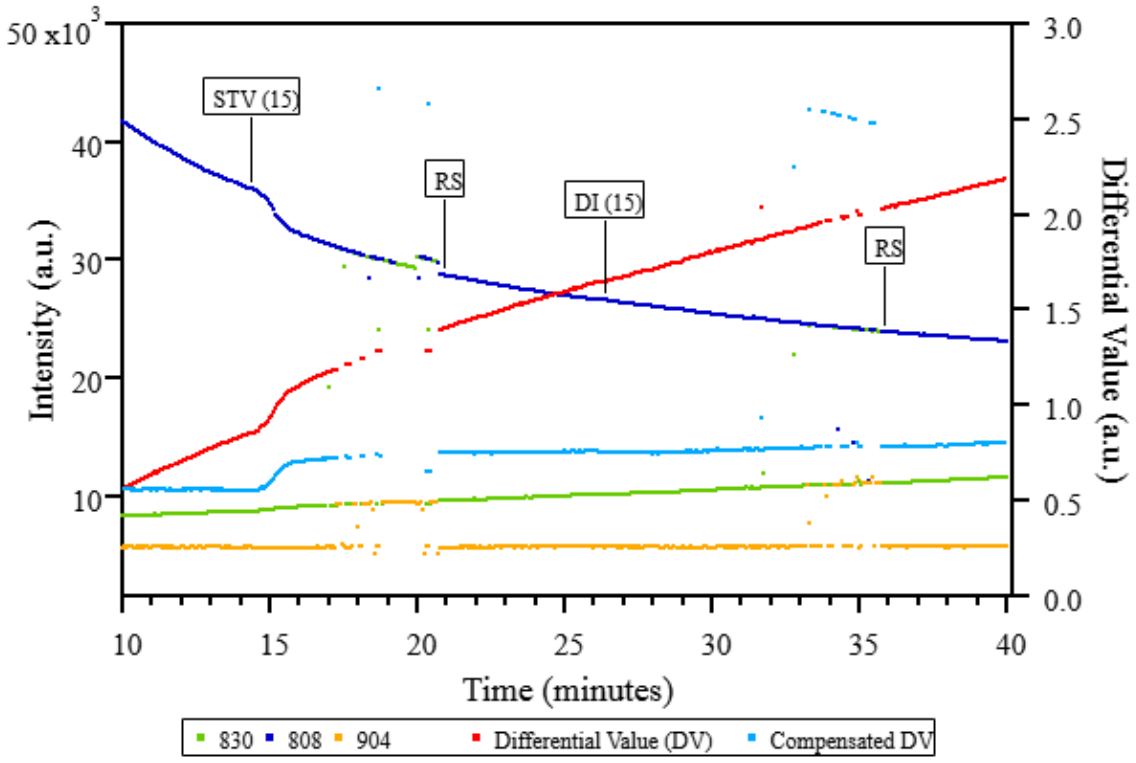

Figure 17: Demonstration of streptavidin adsorption in the first sample. 15 µL of streptavidin (STV) was introduced at 14 minutes. Resynchronization (RS) was done at 21 minutes, since multiple intensities were being recorded on one image from 17-21 minutes. 15 µL of DI water was introduced to rinse at 26.5 minutes, and another RS was performed at 36 minutes.

The same test was performed for another sample with a slightly larger cavity width of 8.36 µm, sample 7. The measurement condition was observed within five minutes of swelling for this sample. After five minutes, 830 nm and 904 nm intensities were used; the 904 nm intensity increased slightly from 5,476 to 5,503 but is still in a

valley region, while the 830 nm intensity rapidly dropped from 28,251 to 9,465 over 50 minutes. The differential increased from 0.677 to 0.867 for a total change of 0.191 over 26 minutes, as shown in Figure 18. There is oscillation from the 830 nm intensity, which may be attributed to fluctuations in current supplied to the laser, or insufficient warm up time before the test. The differential response is more than three times greater in magnitude than the oscillation before streptavidin is introduced. As the differential value increased, the noise increased while streptavidin was incubated. After the DI water rinse, however, the intensity returns to normal. The differential averages were extracted from before and after streptavidin introduction, so the oscillation seen in the incubation period did not affect the differential value change. Again, in this experiment, some residual binding activity is seen after the DI water rinse at 42 minutes.

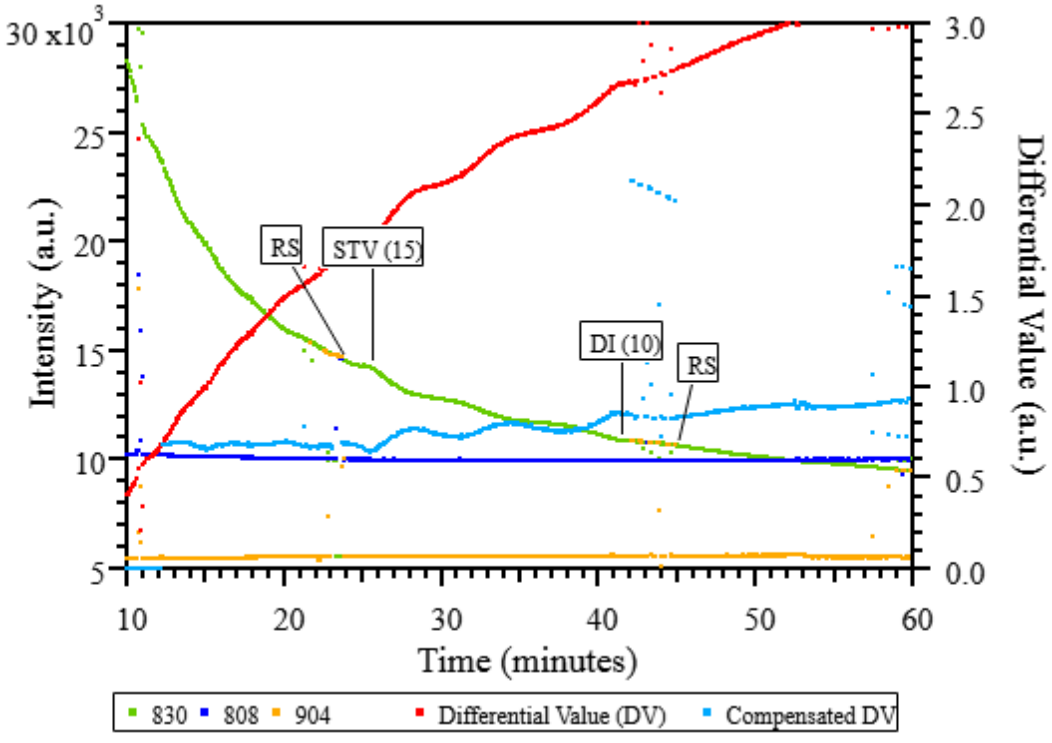

Figure 18: Cavity response for the second streptavidin Test

The differential change of each cavity may also be compared to the simulated differential change for streptavidin bonding. The size of streptavidin is around 4.2 nm × 4.2 nm × 5.6 nm [37], while biotin's size is negligible in comparison. Ideally the silane monolayer of APTES formed on the surface is expected to be about 0.6 nm for vapor phase deposition [36]. Therefore, the total expected thickness of the sensing layer formed on the surface is between 0 to 6.2 nm, for a differential change of 0 to 0.151. It is important to note that streptavidin may not uniformly or completely coat the biotinylated channel; poor passivation or low biotin coverage on the channel can also contribute to a lower average thickness. In addition, a monolayer is not guaranteed. For the differential values in both experiments, 0.228 and 0.191, the estimated sensing layer thicknesses would be 9 nm and 8 nm, respectively, for an 8 μm cavity. These are both at or above the expected change due to streptavidin binding. There were no changes to the functionalization process used from the two-laser system, so the response similar to the two laser tests is expected. Table 5 shows the differential changes and expected layer thicknesses based on the differential change for an 8 μm cavity width for the two samples in this work. Data for the two-laser system using the same concentration is also included for comparison.

Table 5: Differential changes for STV tests.

Sample	Differential Change	Approximate Sensing Layer (nm)
2-A	0.122	5.0
2-B	0.094	3.9
3-A	0.228	9.0
3-B	0.191	7.7
Simulation	0.151	6.2

The differential change appears more sensitive in the most recent two experiments with three wavelengths, 3-A and 3-B. Over the time of exposure to DI water, it is possible that the passivation and biotinylation quality suffers. For shorter swelling and test time, passivation and biotinylation are fresh, allowing streptavidin to bind more efficiently. In addition, it is possible that a monolayer did not form and extraneous APTES or STV molecules were bound to each other. Some variations in molecule size for streptavidin may also be attributed to conformational changes that happen during adsorption [34].

Analysis of SU8 Swelling to Determine Experimental Cavity Width

The aforementioned swelling rate and amount could be determined using the test data and approximate efficiency change per nm change in the cavity. It was evident that each laser shifted by a fixed RIU/nm in simulation; and using this rate the swelling amount and original cavity width could be determined for each fluid test. In addition, the amount of swelling that occurred during these two tests was calculated. The estimated swelling amounts are tabulated below. The post-test cavity width was measured using a profilometer after swelling tests. The swelling amount was estimated using previous optical cavity simulations, by matching the efficiency change in the experiment to the efficiency changes in simulation. From this, the pre-test cavity width may be estimated.

Table 6: Swelling amounts and cavity widths estimated based on intensity responses.

Sample	Total Swelling (nm)	Post-test CW (μm)	Pre-Test CW (μm)
A	18	8.00	7.82
B	24	8.36	8.12

CHAPTER FIVE

Conclusions and Future Work

The benefits of adding a third laser wavelength to the current two-laser optical cavity biosensor were simulated and demonstrated in this thesis. The fabrication tolerance was demonstrably increased by 40 nm in simulations, from 30 nm to 70 nm. It was anticipated that this would widen the window for measurable conditions thus reducing the possible swelling time, and increase the success rate of optical cavity samples. However, despite a much larger fabrication error of 990 nm, measurement conditions were still met in less time than with the two-laser approach. Most samples reached the conditions for a success rate of 88%. Multiple pairs of wavelengths' intensity changes were usable over this variation as well, whereas that much variation in the two-laser system was not usable. For a fabrication error of only 107 nm in the two-laser system samples, only 13 of 16 reached measurement conditions for a success rate of 81%. The fabrication error is considered rather than the fabrication tolerance; due to the inconsistent nature of swelling, the exact cavity widths before testing could not be extracted, only estimated.

The priming time needed for biodetection tests was shortened and made more consistent. Before, the swelling could take 7.71 hours on average, ranging from 0 to 23 hours. With the expansion of the usable range using a third wavelength, 7 of 8 samples were ready to use within 20 minutes, for an average of 4.29 minutes. This drastically reduces the time and materials needed to perform testing, in keeping with the needs for rapid and real time biosensing in medicine. The usability of the device as a biosensor was also demonstrated to have a superior differential response in streptavidin biodetection

tests, despite a wider fabrication error. The differential changes reported in the three-laser system streptavidin detection tests were 0.228 and 0.191, while those reported for the three-laser system were 0.122 and 0.094.

Future Work

More optimization is planned for the three-laser optical cavity-based biosensor, taking further steps toward becoming a point-of-care diagnostic device. Future experiments where the cavity width is measured before testing is crucial to determine the exact fabrication tolerance, rather than the variation. The experimental fabrication tolerance may in fact be much wider for either system, considering there are multiple sets of peaks that may appear over a range of cavity widths. In the previous experiments, the fabrication error being wider than the expected tolerance is indicative of there being more than one cavity width solution to this design. However, fluid flow rate was not a controllable parameter in the above experiments due to the variation in the vacuum pump and the cavity width. The fluid flow rate, which is reduced when the cavity width is decreased, directly increases the incubation time allowed in the sensing area. Fluctuations in the flow rate also occur in the same experiment, attributed to the vacuum pump. In future experiments controlling flow rate may be implemented to better control the incubation time allowed in biodetection experiments, which in turn will improve future sensitivity and limit of detection (LOD) values.

The three-laser system will also be evaluated further under sensitivity and LOD experiments. The success rate and reduced test times will greatly improve the ease of use in further research with minimizing the biosensor to a portable system, and eventual

commercialization. The author was also involved in the development of a portable version of the optical cavity-based biosensor. This system was fabricated from off-the-shelf optical and electrical components mounted in 3D-printed housing, for less than $1,300, a fraction of the cost of facilities and tests from current practice. The two-laser portable system has been successful in refractive index measurements [23]; the next phase would be incorporating the third wavelength for that system as well. In the scope of commercialization, the priming sequence may be completed before the cavity reaches the user, while manufacturing. This phase taking no more than 20 minutes rather than overnight would expedite manufacturing and limit material costs associated with the procedure. The portable system cost less than $1,300 and adding a third wavelength would limit the cost of materials and labor associated with making the optical cavity sample used within it.

Author's Contributions to this project

Since becoming a part of Bio & Micro Devices Lab team at the Baylor Research and Innovation Collaborative (BRIC), the author has contributed:

- As an undergraduate research assistant (URA), fabrication of a portable optical cavity-based biosensor (OCB) of the two-laser system, using commercially available optics and electronics housed in a 3D printed structure. This was used to demonstrate the OCB's capabilities in refractive index sensitivity, as compared to similar tests on the tabletop system. The housing was designed specifically to each component used in SolidWorks, and plastic enclosure was built by hand. The overall dimensions of the portable system were 6.5 in × 8.5 in × 11 in.

- As a URA, co-authored a journal article of the experiments using the portable OCB mentioned above, in 2019.
- Co-authored a review paper, “Label-Free Optical Resonator-Based Biosensors” published in MDPI Sensors in 2020.
- Simulated the performance of the three-laser optical cavity-based biosensor system in terms of fabrication tolerance and expected transmission over cavity widths ranging 7.95-9.20 μm, which are used in this thesis and may also be used in future modifications to the device.
- Fabrication of optical cavity samples (OCSs) and demonstration of the three-laser system to have a higher success rate, larger fabrication error allowance, and superior differential response than with the two-laser approach through preliminary biodetection tests using streptavidin-biotin affinity.
- Trained incoming undergraduate and graduate students who joined the project either as summer interns, senior design teams, or as graduate research assistants on the project since 2018 on a wide variety of topics: 3D printing design, microfabrication and other related functions of developing the optical system.

APPENDIX

APPENDIX A – Two and Three Laser test records and metrics

Test date	Channel	Swelling time - mins	Swelling Time - Hours	Test time - mins	Test Time - Hours	Success count	Notes
5/7/2020	A	100	1.67	188	3.13	N/A	exclude, not same test procedure
	B	Not recorded (NR)	NR	107	1.78	N/A	exclude, not same test procedure
5/10/2020	A	110	1.83	145	2.42	N/A	exclude, not same test procedure
	B	NR	NR	115	1.92	N/A	exclude, not same test procedure
5/14/2020	A	550	9.17	94	1.57	N/A	exclude, not same test procedure
	B	500	8.33	NR	NR	N/A	exclude, not same test procedure
5/17/2020	A	306	5.10	89	1.48	N/A	exclude, not same test procedure
	B	294	4.90	90	1.50	N/A	exclude, not same test procedure
5/21/2020	A	430	7.17	44	0.73	1	
	B	255	4.25	33	0.55	1	
5/25/2020	A	640	10.67	33	0.55	1	8.217
	B	NA	NA	NA			Didn't reach condition
5/27/2020	A	0	0.00	43	0.72	1	
	B	NA	NA	NA			Didn't reach condition
5/29/2020	A	660	11.00	41	0.68	1	8.189
	B	470	7.83	32	0.53	1	
5/31/2020	A	985	16.42	36	0.60	1	8.11
	B	NA	NA	NA			Didn't reach condition
6/6/2020	A	1380	23.00	35	0.58	1	8.13
	B	20	0.33	33	0.55	1	
6/8/2020	A	640	10.67	35	0.58	1	
	B	500	8.33	27	0.45	1	
6/10/2020	A	0	0	30	0.50	1	
	B	35	0.58	28	0.47	1	

Metrics		
Avg. Priming time	7.71	hrs
St. Dev.	6.92	hrs
Avg. Test time	34.62	min
St. Dev.	5.32	min
Succes Count	13	of 16
Success Rate	81%	

Test date	Channel	Swelling time - min	Swelling time - hours	Test Time - min	Cavity Width	Success Count	Notes
2/1/2021	A	0	0.00	25	9.17	1	Exclude, not same fabrication
2/9/2021	A	0	0.00		9.06	1	Exclude, not same fabrication
2/21/2021	A	NA	N/A	N/A	8.47		air introduced, not able to swell
	B	10	0.17	N/A	8.44	1	
3/1/2021	B	20	0.33	N/A	8.99	1	
3/4/2021	A	0	0.00	N/A	8.18	1	air introduced after swelling
	B	0	0.00	30	8.18	1	
3/11/2021	B	0	0.00	26	8.00	1	
3/17/2021	A	0	0.00	28	8.36	1	
	B	0	0.00	NA	8.30	1	air introduced after swelling

Metrics		
Avg. Priming time	4.29	min
St. Dev.	7.87	min
Avg. Test time	27.00	min
St. Dev.	2.00	min
Succes Count	7	of 8
Success Rate	88%	

REFERENCES

[1] M. a. R. Roser, H., "Cancer," C. D. b. Type, Ed., ed. Online: OurWorldInData.org, 2015.

[2] H. Sung *et al.*, "Global cancer statistics 2020: GLOBOCAN estimates of incidence and mortality worldwide for 36 cancers in 185 countries," *CA: A Cancer Journal for Clinicians,* 2021, doi: 10.3322/caac.21660.

[3] A. C. Society. "Lung Cancer Detection, Diagnosis and Staging." American Cancer Society. https://www.cancer.org/cancer/lung-cancer/detection-diagnosis-staging/survival-rates.html.

[4] A. A. Laviana, A. N. Luckenbaugh, and M. J. Resnick, "Trends in the Cost of Cancer Care: Beyond Drugs," *Journal of Clinical Oncology,* vol. 38, no. 4, pp. 316-322, 2020, doi: 10.1200/jco.19.01963.

[5] IUPAC, "Compendium of Chemical Terminology," 2nd ed ed: Blackwell Scientific Publications, Oxford, 1997.

[6] S. P. Mohanty and E. Kougianos, "Biosensors: a tutorial review," *IEEE Potentials,* vol. 25, no. 2, pp. 35-40, 2006, doi: 10.1109/mp.2006.1649009.

[7] N. J. Ronkainen, H. B. Halsall, and W. R. Heineman, "Electrochemical biosensors," *Chemical Society Reviews,* vol. 39, no. 5, p. 1747, 2010-01-01 2010, doi: 10.1039/b714449k.

[8] M. Rao, K. Kapila, and R. Gupta, "ENZYME LINKED IMMUNOSORBENT ASSAYS REVISITED," *Medical Journal Armed Forces India,* vol. 53, no. 1, pp. 45-51, 1997, doi: 10.1016/s0377-1237(17)30644-5.

[9] ThermoFisher. "Overview of ELISA." Thermo Fisher Scientific. https://www.thermofisher.com/us/en/home/life-science/protein-biology/protein-biology-learning-center/protein-biology-resource-library/pierce-protein-methods/overview-elisa.html (accessed 2021).

[10] Y. Yao, B. Yi, J. Xiao, and Z. Li, "Surface Plasmon Resonance Biosensors and its Application," in *International Conference on Bioinformatics and Biomedical Engineering (ICBBE)*, Wuhan, China, 2007 2007: IEEE, doi: 10.1109/icbbe.2007.270. [Online]. Available: https://ieeexplore.ieee.org/document/4272754/

[11] Y. Tang, X. Zeng, and J. Liang, "Surface Plasmon Resonance: An Introduction to a Surface Spectroscopy Technique," *J Chem Educ,* vol. 87, no. 7, pp. 742-746, Jul 2010, doi: 10.1021/ed100186y.

[12] V. S. Ilchenko and A. B. Matsko, "Optical resonators with whispering-gallery modes-part II: applications," *IEEE Journal of Selected Topics in Quantum Electronics,* vol. 12, no. 1, pp. 15-32, 2006, doi: 10.1109/jstqe.2005.862943.

[13] A. B. Matsko and V. S. Ilchenko, "Optical resonators with whispering-gallery modes-part I: basics," *IEEE Journal of Selected Topics in Quantum Electronics,* vol. 12, no. 1, pp. 3-14, 2006, doi: 10.1109/jstqe.2005.862952.

[14] G. C. Righini and S. Soria, "Biosensing by WGM Microspherical Resonators," *Sensors (Basel),* vol. 16, no. 6, Jun 17 2016, doi: 10.3390/s16060905.

[15] D. Rho, C. Breaux, and S. Kim, "Label-Free Optical Resonator-Based Biosensors," *Sensors,* vol. 20, no. 20, p. 5901, 2020, doi: 10.3390/s20205901.

[16] N. Ismail, C. C. Kores, D. Geskus, and M. Pollnau, "Fabry-Perot resonator: spectral line shapes, generic and related Airy distributions, linewidths, finesses, and performance at low or frequency-dependent reflectivity," *Opt Express,* vol. 24, no. 15, pp. 16366-89, Jul 25 2016, doi: 10.1364/OE.24.016366.

[17] A. Syahir, K. Usui, K.-Y. Tomizaki, K. Kajikawa, and H. Mihara, "Label and Label-Free Detection Techniques for Protein Microarrays," *Microarrays,* vol. 4, no. 2, pp. 228-244, 2015-04-24 2015, doi: 10.3390/microarrays4020228.

[18] C. I. L. Justino, T. A. Rocha-Santos, A. C. Duarte, and T. A. Rocha-Santos, "Review of analytical figures of merit of sensors and biosensors in clinical applications," *TrAC Trends in Analytical Chemistry,* vol. 29, no. 10, pp. 1172-1183, 2010-11-01 2010, doi: 10.1016/j.trac.2010.07.008.

[19] I. M. White and X. Fan, "On the performance quantification of resonant refractive index sensors," *Optics express,* vol. 16, no. 2, p. 1020, 2008, doi: 10.1364/OE.16.001020.

[20] M. Taleuzzaman, "Limit of Blank (LOB), Limit of Detection (LOD), and Limit of Quantification (LOQ)," *Organic and Medicinal Chemistry International Journal,* vol. 7, no. 5, p. 5, 2018, doi: 10.19080/OMCIJ.2018.07.555722.

[21] Y. V. H. Ricard Boqué. "The Limit of Detection." LCGC Europe. https://www.chromatographyonline.com/view/limit-detection (accessed 08/30/2020, 2020).

[22] D. E. Brunetti B, "About Estimating the Limit of Detection by the Signal to Noise Approach," *Pharmaceutica Analytica Acta,* vol. 06, no. 04, 2015, doi: 10.4172/2153-2435.1000355.

[23] D. Rho, C. Breaux, and S. Kim, "Demonstration of a Low-Cost and Portable Optical Cavity-Based Sensor through Refractive Index Measurements," *Sensors,* vol. 19, no. 9, May 12 2019, doi: 10.3390/s19092193.

[24] D. Rho and S. Kim, "Demonstration of a Label-Free and Low-Cost Optical Cavity-Based Biosensor Using Streptavidin and C-Reactive Protein," *Biosensors (Basel),* vol. 11, no. 1, Dec 24 2020, doi: 10.3390/bios11010004.

[25] D. Rho, S. Cho, C. Joy, and S. Kim, "Demonstration of an optical cavity sensor with a differential detection method by refractive index measurements," in *2015 Texas Symposium on Wireless and Microwave Circuits and Systems (WMCS)*, 2015-04-01 2015: IEEE, doi: 10.1109/wmcas.2015.7233217.

[26] D. Rho and S. Kim, "Large dynamic range optical cavity based sensor using a low cost three-laser system," in *2017 39th Annual International Conference of the IEEE Engineering in Medicine and Biology Society (EMBC)*, 2017-07-01 2017: IEEE, doi: 10.1109/embc.2017.8037093.

[27] J. Brake and S. Kim, "An optical cavity based biosensor with chained differential detection to improve sensitivity and fabrication tolerance," in *SPIE BiOS*, San Francisco, California, United States, 2014.

[28] D. Rho and S. Kim, "Label-free real-time detection of biotinylated bovine serum albumin using a low-cost optical cavity-based biosensor," *Opt Express,* vol. 26, no. 15, pp. 18982-18989, Jul 23 2018, doi: 10.1364/OE.26.018982.

[29] C. J. Robin and K. N. Jonnalagadda, "Effect of size and moisture on the mechanical behavior of SU-8 thin films," *Journal of Micromechanics and Microengineering,* vol. 26, no. 2, 2016, doi: 10.1088/0960-1317/26/2/025020.

[30] "C-Reactive Protein (CRP) Test." MedlinePlus. https://medlineplus.gov/lab-tests/c-reactive-protein-crp-test/

[31] MayoClinic. "C-reactive protein test." Mayo Foundation for Medical Education and Research (MFMER). https://www.mayoclinic.org/tests-procedures/c-reactive-protein-test/about/pac-20385228 (accessed 2021).

[32] J. Voros, "The density and refractive index of adsorbing protein layers," *Biophys J,* vol. 87, no. 1, pp. 553-61, Jul 2004, doi: 10.1529/biophysj.103.030072.

[33] A. K. Mudraboyina and J. Sabarinathan, "Protein binding detection using on-chip silicon gratings," *Sensors (Basel),* vol. 11, no. 12, pp. 11295-304, 2011, doi: 10.3390/s111211295.

[34] Y. Li and H. Zhang, "Binding of streptavidin to surface-attached biotin with different spacer thicknesses," *Journal of Wuhan University of Technology-Mater. Sci. Ed.,* vol. 30, no. 6, pp. 1304-1309, 2015-12-01 2015, doi: 10.1007/s11595-015-1312-5.

[35] T. Yoshida, M. Nagao, H. Ohsaki, T. Shimizu, and S. Kanemaru, "Densification of spin-on-glass (SOG) film by RF plasma treatment," *IOP Conference Series: Materials Science and Engineering,* vol. 18, no. 3, 2011, doi: 10.1088/1757-899x/18/3/032007.

[36] M. Zhu, M. Z. Lerum, and W. Chen, "How To Prepare Reproducible, Homogeneous, and Hydrolytically Stable Aminosilane-Derived Layers on Silica," *Langmuir,* vol. 28, no. 1, pp. 416-423, 2012-01-10 2012, doi: 10.1021/la203638g.

[37] E. H. Williams *et al.*, "Immobilization of streptavidin on 4H–SiC for biosensor development," *Applied Surface Science,* vol. 258, no. 16, pp. 6056-6063, 2012, doi: 10.1016/j.apsusc.2012.02.137.